Pore Scale Study on Dissociation and Transportation of Methane Hydrate

Xiaowei Zhang, Yanlong Guan, and Yudou Wang *

School of Science, China University of Petroleum (East China), Qingdao, 266580, China

Abstract. Methane hydrate, recognized as a promising clean energy resource, undergoes complex multiphase dynamics during dissociation, involving intricate interactions between fluid flow, heat transfer, and mass transport phenomena. It is crucial to explain its physical behavior in the dissociation process from the pore scale. This paper proposes an improved flow model, which simulated the dissociation process of methane hydrate at pore scale. As the first effort in literature, the characteristics of hydrate domain are considered to better reproduce the multiphase flow, heat and mass transfer behavior. The evolution of flow velocity, temperature and saturation was simulated. The results indicate that the improved flow model, based on the Darcy-Brinkman-Stokes equation, can accurately replicate the multiphase flow transfer, heat, and mass transport phenomena during hydrate dissociation. Furthermore, the flow characteristics of hydrate domain significantly influence methane extraction efficiency. This study offers novel insights into pore-scale modeling of multiphase flow systems involving phase change phenomena.

Keywords: Methane hydrate; Pore scale model; Dissociation; Multiphase flow; Heat and mass transfer.

1. Introduction

Methane hydrate, recognized as a promising unconventional natural gas resource, is predominantly distributed in two distinct geological settings: marine continental margins and terrestrial permafrost sediments, where specific pressure and temperature conditions prevail. Investigation of its dissociation mechanisms holds significant implications across multiple scientific disciplines, including energy resource development, environmental sciences, and geophysical research, making it a crucial area of study in contemporary earth sciences [1, 2].

The dissociation of methane hydrate involves mass transfer, heat transfer, and chemical reaction. The process of dissociation can change pore structure in porous media, and the transports properties will be modified by the dynamic evolution of pore structure in turn [3]. It is a complicated multiphase and multi-component flow process. Elucidating the dissociation mechanisms of methane hydrate at the microscopic scale is crucial for developing efficient extraction technologies. Pore-scale investigations of methane hydrate dissociation significantly enhance our understanding of multiphase flow dynamics in hydrate-bearing sediments [4]. Furthermore, the development of advanced pore-scale models for hydrate dissociation kinetics not only facilitates the optimization of gas production strategies but also contributes to the mitigation of potential seafloor geological hazards associated with hydrate exploitation.

Due to the unpredictable nature of hydrate formation and dissociation locations, coupled with the challenging experimental conditions, significant discrepancies persist in pore-scale experimental studies, and a unified understanding has yet to be established. Consequently, numerous researchers have turned to numerical simulations to investigate the dissociation behavior of hydrates. Sean et al. [5] developed a comprehensive pore-scale model utilizing Computational Fluid Dynamics (CFD) to simulate methane hydrate dissociation. Their approach established the Gibbs free energy difference between the hydrate and surrounding aqueous phase as the primary dissociation driving force, while assuming complete methane dissolution in water to characterize dissociation processes within the fluid domain. Subsequently, Zhang et al. [6] introduced a single-phase flow pore-scale model for hydrate dissociation using the Lattice Boltzmann Method (LBM). Their model incorporated temperature variations induced by heat transfer mechanisms, which significantly influenced dissociation kinetics, and established permeability as a function of methane hydrate saturation in

porous media. However, this study was limited by its exclusive focus on single-phase flow, neglecting the critical dynamics of both methane gas and water flow. Advancing the field further, Song et al. [7] implemented the Volume of Fluid (VOF) method to construct a sophisticated pore-scale model for methane hydrate dissociation. Their investigation provided valuable insights into the complex interactions of multiphase flow, heat transfer, and mass transfer within pore spaces, while deriving normalized permeability values across varying hydrate saturation levels, representing a significant contribution to pore-scale modeling methodologies. In addition, Yang et al. [8] simulated the multiphase flow, heat and mass transfer, and structural evolution of hydrates during the hydrate dissociation process based on the LBM method. They proposed an empirical model of permeability and specific surface area and improved the REV-scale modeling. However, a significant limitation in previous studies is the treatment of hydrates as solid entities, which fails to account for the fluid flow characteristics within hydrate structures. In reality, hydrates can be more accurately represented as permeable porous media governed by Darcy flow, while the surrounding fluid domain follows Stokes flow principles. During the dissociation process, the Darcy flow domain progressively diminishes until complete hydrate dissociation is achieved. This dynamic process necessitates careful consideration of the mass and energy transfer mechanisms between the internal and external fluid domains. The Darcy-Brinkman-Stokes (DBS) equation [9] has been implemented to effectively couple the Navier-Stokes flow in the fluid domain with Darcy flow in the hydrate-bearing porous media, providing a comprehensive framework for modeling flow behavior in hydrate reservoir pore spaces.

This study develops an advanced pore-scale numerical model for methane hydrate dissociation, incorporating the DBS equation to enhance gas recovery prediction accuracy. The model's validity is systematically validated through comprehensive comparisons with established numerical benchmarks. The proposed simulation framework provides detailed insights into the complex interplay of multiphase flow dynamics, coupled heat transfer mechanisms, and mass transport phenomena during the dissociation of pore-scale hydrate-bearing sediments.

2. Mathematical model

2.1 Kinetics reaction model of hydrate dissociation

The dissociation process of methane hydrate can be modeled as:

$$CH_4 \cdot nH_2O \rightarrow CH_4 + nH_2O \quad (1)$$

In this study, the average number of water molecules in methane hydrate is denoted as n, with n = 6 being the specific value adopted. The kinetic equation governing methane hydrate dissociation was originally established by Kim et al. [10] through comprehensive experiments conducted in a stirred-tank reactor in 1987. The equation is expressed as follow:

$$m_h = -k_0 e^{-\frac{E}{(RT)}} M_h A_s (Pe - p) \quad (2)$$

Where k_0 is the intrinsic constant ($mol/m^2 \cdot Pa \cdot s$), E is the activation energy (J), R is the universal gas constant ($J/mol \cdot K$), T is the temperature, M_h is the molecular weight (kg/mol) of hydrate. A_s is the reaction specific surface of hydrate ($1/m$). p is the gas pressure (MPa). Pe represents equilibrium pressure (MPa) which is defined as follow [11]:

$$Pe = 1.15e^{49.3185-\frac{9459}{T}} \quad (3)$$

The reaction rates for methane and water generation during the hydrate dissociation process are expressed as follows, respectively:

$$m_g = k_0 e^{-\frac{E}{(RT)}} A_s M_g (Pe - p) \quad (4)$$

$$m_w = 6k_0 e^{-\frac{E}{(RT)}} A_s M_w (Pe - p) \quad (5)$$

Where M_g, M_w are the molecular weight (kg/mol) of methane and water, respectively.

2.2 Darcy-Brinkman-Stokes model for multiphase flow

The multiphase model developed in this study encompasses gas, water, and hydrate phases. To characterize the mass transport phenomena during hydrate dissociation, the phase saturation is quantitatively described through the following expression:

$$\sum_{i=h,w,g} S_i = 1 \quad (6)$$

Where S_h , S_w , S_g represent hydrate saturation, water saturation, methane saturation, respectively.

The dissociation process within microscopic pore structures, which are distinctly partitioned into hydrate and fluid domains, induces a dynamic redistribution of both phase distributions. As dissociation proceeds, this phase reconFigureuration substantially modifies the spatial arrangement and connectivity of the hydrate and fluid phases. Within the fluid domain, flow dynamics are mathematically described by the Navier-Stokes equations. Conventionally, hydrate structures have been treated as impermeable solid phases, precluding any fluid transport through the hydrate matrix. However, emerging experimental evidence [12,13] has demonstrated the occurrence of mass transport phenomena within hydrate structures, significantly impacting the dissociation kinetics. In the present study, we conceptualize the hydrate domain as a porous medium, with fluid transport characteristics governed by Darcy's law.

Given that hydrate phases remain stationary while methane exhibits solubility in water and consequently migrates at identical velocities to the aqueous phase, the fluid dynamics can be effectively characterized by the Darcy-Brinkman-Stokes (DBS) equation, formulated as follows:

$$\rho\frac{\partial u}{\partial t} + \rho(\nabla \cdot u)u = -\nabla p + \mu\nabla^2 u - \mu\frac{1}{k}u + F \quad (7)$$

Where ρ, μ, u, p, F represent the density (kg/m^3), viscosity ($Pa \cdot s$), pressure (MPa), velocity (m/s) and bulk force (N). In equation (7), inertia forces are on the left hand, while the viscous forces and bulk forces are on the right hand. The density ρ and viscosity μ are given as follows:

$$\rho = \sum_{i=h,w,g} S_i\rho_i \quad (8)$$

$$\mu = \sum_{i=w,g} S_i\mu_i \quad (9)$$

Where ρ_i, μ_i represent density and dynamic viscosity of the ith phases. Since the permeability k of hydrate domain follows Kozeny-Carman (KC) model [14]. When the hydrate is completely dissociation, the permeability k is large enough so that the Eq (7) can be written as the Navier-Stokes equation as follows:

$$\rho\left(\frac{\partial u}{\partial t} + (u \cdot \nabla)u\right) = -\nabla p + \mu\nabla^2 u + F \quad (10)$$

2.3 Mass and heat transport model

Considering the immobile nature of the hydrate phase, the mass conservation equation can be expressed as follows (Eq. 11):

$$\frac{\partial \rho_h S_h}{\partial t} + k_0 e^{-\frac{E}{(RT)}} M_h A_s (Pe - p) = 0 \quad (11)$$

While the mass conservation equations of the fluid domain are given by Eq. (12) and Eq. (13):

$$\frac{\partial \rho_g S_g}{\partial t} + \nabla \cdot (\rho_g S_g u) - k_0 e^{-\frac{E}{(RT)}} M_g A_s (Pe - p) = 0 \quad (12)$$

$$\frac{\partial \rho_w S_w}{\partial t} + \nabla \cdot (\rho_w S_w u) - 6k_0 e^{-\frac{E}{(RT)}} M_w A_s (Pe - p) = 0 \quad (13)$$

During the dissociation of methane hydrate, the energy conservation equations governing the hydrate and fluid domains can be expressed as follows:

$$\rho C\frac{\partial T}{\partial t} + \rho Cu \cdot \nabla T + \nabla \cdot (k\nabla T) = Q \quad (14)$$

Where k, C represent thermal capacity ($J/(kg \cdot K)$) and effective thermal conductivity ($W/(m \cdot K)$), which are given as follows:

$$k = \sum_{i=h,w,g} S_i k_i \quad (15)$$

$$C = \sum_{i=h,w,g} S_i C_i \quad (16)$$

In Eq. (14), the reaction heat source of hydrate ($J/m^3 \cdot s$) is represented by Q, which is written as follows:

$$Q = m_h \Delta H \quad (17)$$

Where m_h is the hydrate reaction rate ($kg/(m^3 \cdot s)$), ΔH represents the reaction enthalpy (J/kg).

Given the absence of fluid velocity and heat source terms in sand grains, the energy conservation equation can be formulated as follows:

$$\rho_s C_s \frac{\partial T}{\partial t} + \nabla \cdot (k_s \nabla T) = 0 \quad (18)$$

Where ρ_s, C_s, k_s represent the density, thermal capacity and effective thermal conductivity of the sand grains.

3. Model validation

To verify the reliability of the proposed model, a comprehensive validation was conducted by comparing our numerical results with the simulation data from Song et al. (2021) [15]. The geometric conFigureuration and physical parameters were rigorously maintained identical to those described in the reference study. Figure 1 presents a comparative analysis of velocity distributions at three distinct time intervals (0.1 s, 25 s, and 50 s). The computational results from this study (Figures. 1a-1c) are juxtaposed with the simulation data reported by Song et al. (Figures. 1d-1f). The analysis reveals a fundamental distinction in the treatment of the hydrate domain: while Song et al.'s model neglects fluid flow characteristics within the hydrate region, our formulation explicitly accounts for these dynamics. Consequently, our results demonstrate measurable velocity distributions within the hydrate domain, with the magnitude increasing progressively during the dissociation process until complete phase transition. Notably, despite this methodological difference, the overall velocity distributions exhibit remarkable consistency between the two studies, particularly in the fluid-dominated regions.

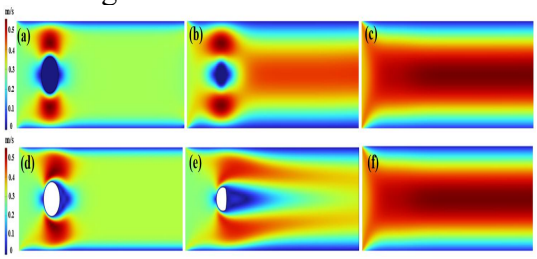

Figure. 1 Distributions of the velocity vectors at the time of 0.1s, 25s, 50s in this study (Figures. 1a-1c) and Song et al. [15] (Figures. 1d-1f).

Figure 2 demonstrates the temporal evolution of hydrate saturation at the hydrate centroid during the dissociation process. The simulation results are presented with the red solid line representing the data from Song et al. and the black solid line corresponding to the computational results obtained in the current study. Comparative analysis reveals a strong correlation between both datasets, with minor discrepancies observed. These variations can be attributed to the incorporation of fluid flow dynamics within the hydrate domain in our model. Specifically, the consideration of fluid presence in the hydrate region results in a marginally slower decrease in hydrate saturation compared to the reference study by Song et al., where such flow characteristics were not accounted for in their formulation.

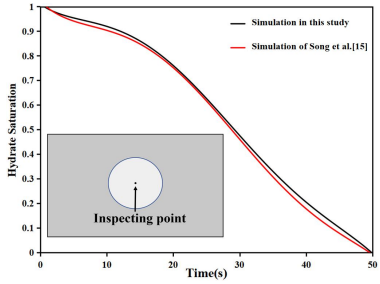

Figure. 2 Comparison of hydrate saturation at the inspecting point (the center of the hydrate domain) for the simulation of Song et al. and the simulation in this study.

4. Application of the model

The parameters used for simulating the dissociation process of hydrate are listed in Table 1.

Table 1. Parameters for the simulation in this study.

Parameter	Symbol	Value	Units
Hydrate density	ρ_h	917	kg/m3
Water density	ρ_w	1000	kg/m3
Methane density	ρ_g	40	kg/m3
Sandy grains density	ρ_s	2650	Kg/m3
Water viscosity	μ_w	1.8E-3	Pa·s
Methane viscosity	μ_g	1E-6	Pa·s
Thermal conductivity of hydrate	k_h	0.393	W/(m·K)
Thermal conductivity of water	k_w	0.6	W/(m·K)
Thermal conductivity of methane	k_g	3.35E-3	W/(m·K)
Thermal conductivity of sandy grains	k_s	0.5	W/(m·K)
Thermal capacity of hydrate	C_h	2010	J/(kg·K)
Thermal capacity of water	C_w	4180	J/(kg·K)
Thermal capacity of methane	C_g	2205	J/(kg·K)
Thermal capacity of sandy grains	C_s	800	J/(kg·K)
Reacting surface of hydrate	A_s	3.75E5	1/m
Intrinsic reaction rate constant	k_0	1.24E5	mol/m2·Pa·s
Reaction enthalpy	ΔH	418210	J/kg
Activation energy	E	78150	J/mol
Universal gas constant	R	8.314	J/mol·K
Molecular weight of hydrate	M_h	0.124	kg/mol
Molecular weight of water	M_w	0.018	kg/mol
Molecular weight of methane	M_g	0.016	kg/mol

Grain-coating (GC) hydrate represents a distinct hydrate endowment morphology characterized by hydrate formation on particle surfaces. Figure 3 presents the geometric conFigureuration and computational mesh of the GC model employed in this study. The two-dimensional domain, measuring 2.8 mm in length and 1.1 mm in width, consists of methane hydrate (indicated in red) and sand grains (shown in white) with a uniform diameter of 0.096 mm. The model incorporates specific boundary conditions: the left boundary serves as the fluid inlet, while the right boundary functions as the fluid outlet. The upper and lower boundaries are constrained by non-slip, adiabatic, impermeable, and non-reactive conditions to simulate realistic reservoir environments. The computational domain was discretized using an unstructured grid system, with distinct mesh resolutions applied to different phases. The fluid domain was partitioned into 8,411 computational cells, featuring cell sizes ranging from 1.74 × 10-4 mm to 1.51 × 10-2 mm. To accurately capture the complex phase change dynamics, the hydrate domain was implemented with a significantly

refined mesh, comprising 46,696 computational cells. This refined grid structure exhibits cell dimensions varying between 2.32×10-5 mm and 7.81×10-3 mm, ensuring adequate resolution for the hydrate dissociation process. The initial thermodynamic conditions were carefully selected to maintain hydrate stability while enabling controlled dissociation. The system was initialized at a temperature (T0) of 272 K, below the equilibrium conditions for hydrate stability. To initiate the dissociation process, injection water was introduced at a temperature (Tin) of 280 K, with a specified inlet velocity (Vin) of 6×10-4 m/s. The initial reservoir pressure (P0) was maintained at 2.64 MPa, ensuring appropriate phase equilibrium conditions throughout the computational domain.

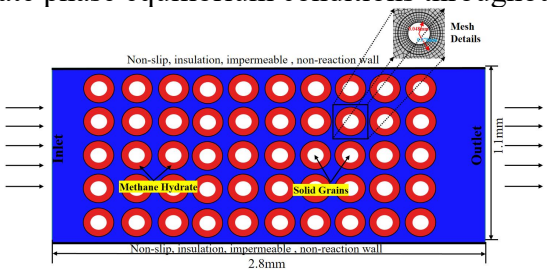

Figure. 3 Geometry and computational domain of grain-coating hydrate model for dissociation simulation.

Figure 4 presents the spatial distribution of flow velocities within the computational domain at three distinct dissociation stages: 0.1 s, 5 s, and 10 s for the dissociation of GC. The results reveal a significant temporal evolution in flow dynamics: during the initial dissociation phase, maximum flow velocities are observed in the primary pore channels. Conversely, the hydrate domain exhibits minimal flow activity at this stage. As the dissociation progresses, a notable transition occurs, characterized by progressively increasing velocities within the hydrate domain. This phenomenon is accompanied by a corresponding decrease in flow velocities through the constricted pore channels, suggesting a redistribution of flow pathways as the hydrate phase transition advances.

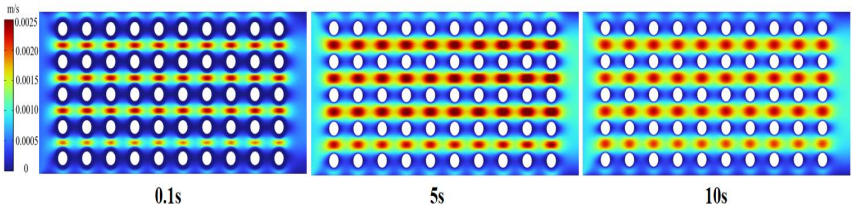

Figure. 4 Simulated distributions of velocity based on DBS equation at 0.1s, 5s, and 10s.

Figures 5 and 6 illustrate the temporal evolution of hydrate saturation and methane saturation during the dissociation process, respectively. The simulation results demonstrate that the injected hot water provides sufficient thermal energy to drive the endothermic dissociation reaction of gas hydrates. The dissociation initiates preferentially in the vicinity of the injection boundary adjacent to the hot water front, accompanied by methane gas generation. The majority of hydrates have dissociated, and the liberated methane migrates toward the production outlet along with the hot water flow at 5s. Complete hydrate dissociation is achieved at 10s. Notably, the model in this study predicts residual methane gas at the simulation endpoint (10s) due to the incorporation of hydrate domain flow characteristics. In contrast, simulations neglecting the flow characteristics show complete methane discharge by 10s under identical conditions.

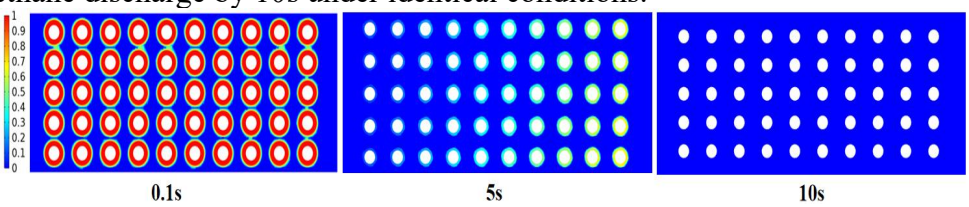

Figure. 5 Simulated distributions of hydrate saturation at 0.1s, 5s, and 10s.

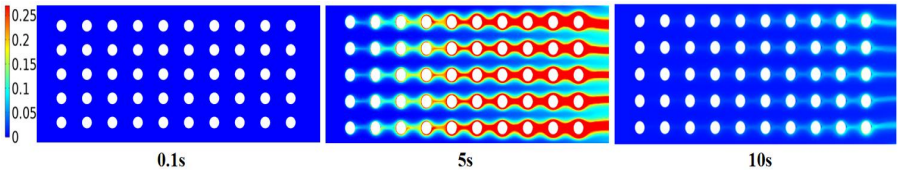

Figure. 6 Simulated distributions of methane saturation at 0.1s, 5s, and 10s.

Figure 7 presents the spatial and temporal evolution of temperature distribution within the model at four distinct time intervals (0.1 s, 2 s, 5 s, and 10 s) during the dissociation process. The results reveal a progressive thermal propagation pattern, characterized by a gradual temperature increase from the injection boundary toward the central region of the domain. This thermal front advancement demonstrates the effective heat transfer mechanism within the system. Notably, the entire domain achieves thermal equilibrium, with the temperature uniformly reaching the injection temperature of the hot water by 10s, indicating complete thermal saturation of the system.

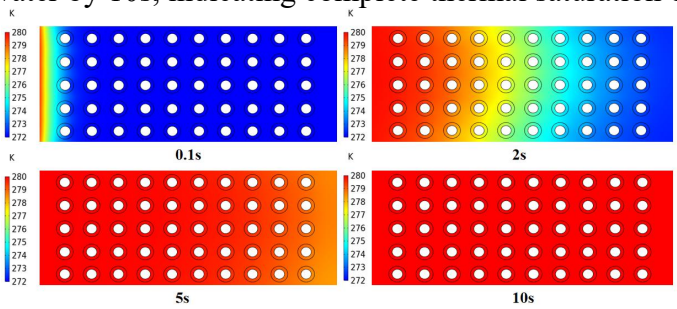

Figure. 7 Simulated distributions of temperature at 0.1s, 2s, 5s, and 10s.

5. Conclusion

This study presents an enhanced pore-scale model for hydrate dissociation, which accurately characterizes multiphase flow dynamics during the dissociation process through the integration of the DBS equation. The following conclusions can be achieved:

The proposed model successfully reproduces phase transitions, temperature evolution, and saturation changes during hydrate dissociation.

2. Preliminary investigations reveal that the flow characteristics within hydrate domains significantly influence methane production efficiency.

However, systematic studies are still required to elucidate: (1). The gas production rates across various hydrate reservoir types. (2). The impact of thermal stimulation parameters, including injection temperature and flow velocity, on methane extraction dynamics. These advancements provide valuable insights into the dissociation kinetics at the pore scale and contribute to the development of efficient hydrate reservoir exploitation strategies.

References

[1] Chen B, Sun H, Zheng J, Yang, M. New insights on water-gas flow and hydrate decomposition behaviors in natural gas hydrates deposits with various saturations. Applied Energy, 2020, 259: 114185.

[2] Chen L, Feng Y, Kogawa T, Okajima J, Komiya A, Maruyama S. Construction and simulation of reservoir scale layered model for production and utilization of methane hydrate: The case of Nankai Trough Japan. Energy, 2018, 143: 128-140.

[3] Cui H, Su X, Liang J, Chen F, Dong P, Hai L. Microbial diversity in fracture and pore filling gas hydrate-bearing sediments at Site GMGS2-16 in the Pearl River Mouth Basin, the South China Sea. Marine Geology, 2020, 427: 106264.

[4] Chen C, Zhang Y, Li X, He J, Gao F, Chen Z. Investigations into methane hydrate formation, accumulation, and distribution in sediments with different contents of illite clay. Applied Energy, 2024, 359: 122661.

[5] Sean WY, Sato T, Yamasaki A, Kiyono F. CFD and experimental study on methane hydrate dissociation Part I. Dissociation under water flow. American Institute of Chemical Engineers Journal, 2007, 53: 262-274.

[6] Zhang L, Zhang C, Zhang K, Zhang L, Yao J, Sun H, Yang Y. Pore‐scale investigation of methane hydrate dissociation using the lattice Boltzmann method. Water Resource, 2019, 55: 8422-8444.

[7] Song R, Liu J, Yang C, Sun S. Study on the multiphase heat and mass transport mechanism in the dissociation of methane hydrate in reconstructed real-shape porous sediments. Energy, 2022, 254: 124421.

[8] Yang J, Xu Q, Liu Z, Shi L. Pore-scale study of the multiphase methane hydrate dissociation dynamics and mechanisms in the sediment. Chemical Engineering Science, 2022, 430: 132786.

[9] Nillama L, Yang J, Yang L. An explicit stabilised finite element method for Navier-Stokes-Brinkman equations. Journal of Computational Physics, 2022, 457: 111033.

[10] Kim H, Bishnoi PR, Heidemann RA. Kinetics of methane hydrate decomposition. Chemical Engineering Science, 1987, 42: 1645-1653.

[11] Sadeq DJ. Gas hydrates investigation: flow assurance for gas production and effects on hydrate-bearing sediments. Journal of Environmental Engineering and Science, 2018.

[12] Li Y, Xu T, Xin X, Xia Y, Zhu H, Yuan Y. Multi-scale comprehensive study of the dynamic evolution of permeability during hydrate dissociation in clayey silt hydrate-bearing sediments. Journal of Hydrology, 2024, 12: 131178.

[13] Feng Y, Qu A, Han Y, Shi C, Liu Y, Zhang L, Zhao J, Yang L, Song Y. Effect of gas hydrate formation and dissociation on porous media structure with clay particles. Applied Energy, 2023, 349: 121694.

[14] Fang M, Tan P, Ward J. Efficient estimation of crystal filterability using the discrete element method and the Kozeny-Carman equation. Powder Technology, 2024, 441: 119820.

[15] Song R, Sun S, Liu J, Yang C. Pore scale modeling on dissociation and transportation of methane hydrate in porous sediments. Energy, 2021, 237: 121630.